Ocean Engineering 286 (2023) 115504

Contents lists available at ScienceDirect

Ocean Engineering

journal homepage: www.elsevier.com/locate/oceaneng

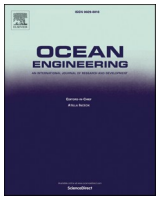

OrcaFlex predictions for a multi-float hinged WEC with nonlinear mooring systems: Elastic mooring force and dynamic motion

Chenyu Zhao [a,*], Peter Stansby [c], Lars Johanning [a,b]

[a] Renewable Energy Group, College of Engineering, Mathematics and Physical Sciences, University of Exeter, UK
[b] Naval Architecture, Harbin Engineering University, Nantong Main Street 145, Nangang District, Harbin, China
[c] School of Engineering, University of Manchester, Manchester, UK

ARTICLE INFO

Handling Editor: Prof. A.I. Incecik

Keywords:
WEC
Nonlinear mooring system
Orcaflex
Numerical method selection
Stiffness properties
Tension reduction

ABSTRACT

The mooring system can affect the motion and energy output characteristics of a WEC. This study investigated the effects of an SPM mooring system in a M4 6-float WEC. The scaled model of M4 was modelled via both Orcaflex and experimental approaches. Compared with experimental results, the accuracy of the numerical results was found to be sensitive to the simulation methods in OrcaFlex, and the filter method supplied a better agreement with experimental results in this study. Following the numerical method selection, another two mooring cables were introduced to compare different stiffness properties with respect to tension reduction. Compared with the other two mooring cables, cable 3 with negative bending has the lowest peak spectral density of tension in all wave conditions; however, its stiffness needs to be optimised to reduce the peak tension in some large wave conditions. According to this, the stiffness of cable 3 is initially adjusted, and the new cable 3 can reduce up to 30% offset distance and 50% peak tension. The results also found that the relative rotational motion of the M4 is not sensitive to stiffness properties, which means the future PTO selection could be independent of the mooring cable.

1. Introduction

Wave energy has significant potential to contribute to the offshore renewable energy industry thanks to its high energy density and widespread distribution (Pacaldo et al., 2022; Shi et al., 2022; Yang et al., 2022). As a result, the wave energy converter (WEC) has sparked considerable research and industry interest, leading to significant developments regarding its structure and working principles (Aderinto and Li, 2018; Ahamed et al., 2020). Many WEC projects have reached a sea trial level close to commercial applications (Antonio, 2010; Liu et al., 2016; López et al., 2013; Sun et al., 2021). However, compared to other offshore renewable technologies, WECs face several challenges, including low capacity and durability (Astariz and Iglesias, 2015; Clément et al., 2002). For instance, the capacity of a typical offshore wind turbine can easily reach 10 MW, yet it is uncommon for a single WEC's capacity to exceed 2 MW. Consequently, large wave energy projects may not always be cost-effective.

In efforts to increase the output power of WECs, more projects are aiming for offshore deployment, providing flexible deployment opportunities and access to more abundant wave energy resources. However, the harsh offshore environment presents significant challenges for the design of the WEC's mooring system. Compared to other offshore structures, the WEC mooring system design is more complex as it needs to consider a wider range of factors, including mooring line dynamics during resonant wave frequencies, water depth, device array effects, and Power Take-Off (PTO) characteristics. For example, an oscillating body WEC typically extracts energy from its relative motion, so an overly rigid mooring system may reduce energy output. Xu et al. (2019) conducted a comprehensive review of different mooring systems in WEC projects and proposed a design process for the WEC mooring system. Given these considerations, the mooring system is often a high-cost element within a wave energy project, accounting for up to 30% of the overall WEC device cost (Thomsen, 2015). Many previous studies have focused on the mooring system selection for the WECs. For example, free hanging catenary/multi-catenary moorings and Catenary Anchor Leg Mooring (CALM) or single anchor leg mooring (SALM) is found to be a better solution for large dimensional WEC (Harris et al., 2004). The hybrid mooring system, including the mooring cable and floaters, performed better than the single moorings in the WEC application (Fonseca et al., 2009; Xu and Soares, 2020).

* Corresponding author.
E-mail address: c.zhao@exeter.ac.uk (C. Zhao).

https://doi.org/10.1016/j.oceaneng.2023.115504
Received 27 March 2023; Received in revised form 16 July 2023; Accepted 29 July 2023
Available online 8 August 2023

Recently, novel mooring components with nonlinear damping properties have been integrated into WECs, demonstrating substantial advantages in tension reduction and device motion stabilisation. In Wang et al. (2022), a passive damper, known as Exeter tether, could reduce up to 67% peak tension and 25% required mooring diameter under the identical mooring configuration. Nonlinear polyester ropes were also recommended in the WEC mooring design owing to their advantages with respect to peak load reduction (Thomsen et al., 2015; Weller et al., 2015a, 2015b). However, the literature has tended to focus on individual nonlinear mooring components, potentially limiting the general applicability of the results. Recent studies on the compatibility between nonlinear damping properties and PTO types have also been limited. This paper investigated the effects caused by a hybrid mooring system in a 6-float attenuator-type WEC known as M4. The University of Manchester research team first promoted the M4 concept, and the early prototype has three floating bodies that extract wave energy from their relative motions (Stansby et al., 2015). Recently, a new M4 with six floaters and two PTOs was tested in an ocean basin testing. The capacity of each PTO can reach 1–2 MW at full scale, potentially increasing further with the addition of more floats and controls (Liao et al., 2021);

This paper can be regarded as an ongoing numerical exploration, building on the experimental study of M4 in 2022, which demonstrated the potential of elastic mooring lines with nonlinear stiffness properties in significantly reducing extreme snap - up to 1/6th of those observed with inelastic cables (Stansby et al., 2022). Nonetheless, it's important to acknowledge that the stiffness of certain materials, such as rubber (Cambridge, 2023), can show substantial variation under different tension or extension ratios. With this consideration, this study also integrated another nonlinear mooring cable, bearing a completely different stiffness curve from the experimental cable (referred to as E2), into the numerical model to further probe the effects of nonlinear mooring cables. Moreover, significant numerical errors were discovered in the Oraflex in the experimental study. As a response to these errors, an alternative simulation approach was selected within Orcaflex to enhance its operational performance.

The remainder of this paper is organised as follows: Section 2 introduces the numerical modelling of the M4 with mooring configurations. Section 3 compares the results from numerical simulations and basin tests. The tension and energy delivered results are introduced in section 4. Section 5 discusses the main findings in light of potential industrial applications and further R&D requirements. Section 6 concludes with the main findings and outcomes.

2. Numerical modelling

This section introduced the simulation approach used in this study, including the numerical model overview and the mooring system configuration.

2.1. Model illustrations

The numerical model, including frequency-domain and time-domain modules, has been used in other authors' studies (Zhao et al., 2021a, 2021b). As presented in Fig. 1, the hydrodynamic coefficients of the single buoy and interaction between multi buoys are calculated by a frequency-domain solver, OrcaWave. The nonlinear forces, such as the mooring and PTO loads, will be considered in the time domain with a solver known as the OrcaFlex (Manual, 2006). The output of this time-domain module includes i) the Hydrodynamic Response of the device, ii) the Tensile load of the mooring system, and iii) the Energy output of the PTO.

Owing to nonlinear forces consideration, the governing equation of the individual float under the time-domain module is presented as:

$$[M+m_\infty]\ddot{\xi}(t)+\int_{-\infty}^{t}H(t-\tau)\dot{\xi}(\tau)d\tau+([V_{vis}])\dot{\xi}(t)+([K])\xi(t)=[F_1(t)]+[F_2(t)]+[F_{moor}]+[F_{PTO}]+[F_c] \quad (1)$$

where $[M+m_\infty]$ is the mass matrix under 6-DOFs (including the added mass matrix for $\omega\rightarrow\infty m_\infty$), $H(t)$ is the retardation function matrix which can be obtained from the convolution integrals of frequency-dependent damping matrix H_d, $[V_{vis}]$ is the viscous damping matrix which is obtained by scaled wave tank experiment (Huang et al., 2018). $[K]$ is the hydrostatic stiffness matrix, ξ is the WEC's displacement matrix, $[F_{moor}]$ is the mooring line's force matrix and $[F_1(t)]$ is the first-order wave force matrix. $[F_2(t)]$ is the second-order force matrix calculated by the far-field formulation. The hydrodynamic coefficients used in eq. (1) have considered contributions and interactions from all 6-DOFs, which are calculated by a boundary solver OrcaWave (Orcina, 2016). $[F_{PTO}]$ and $[F_c]$ are the PTO resistance force and connection forces between multi-buoys. The single float is generalised to multiple floats by constraints in Orcaflex, which can fix/release the motion under individual DoF. For the M4, relative pitch motion between the middle and rear buoys is released.

2.2. Model configuration

2.2.1. M4 scaled model

The OrcaFlex model is constructed based on the physical test of the M4 scaled model, which was tested in the Lir Ocean Basin at University College in Cork, Ireland (Moreno and Stansby, 2019; Stansby et al., 2022). The M4 model was scaled down by a 1:50 ratio in accordance with the Froude principle during the test. The specifications of the M4 scaled model are outlined in Fig. 2. Moreover, the buoy mass listed in Table 1 takes into account the mechanical connection structure. Additional information regarding the basin test configuration and results can be found in the preceding experimental study (Stansby et al., 2022). The

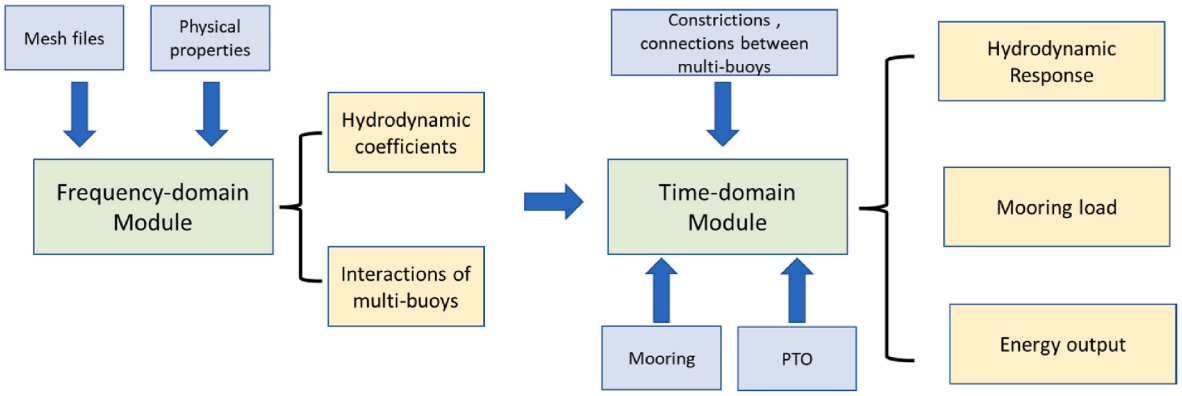

Fig. 1. The numerical model overview includes a frequency- and a time-domain model.

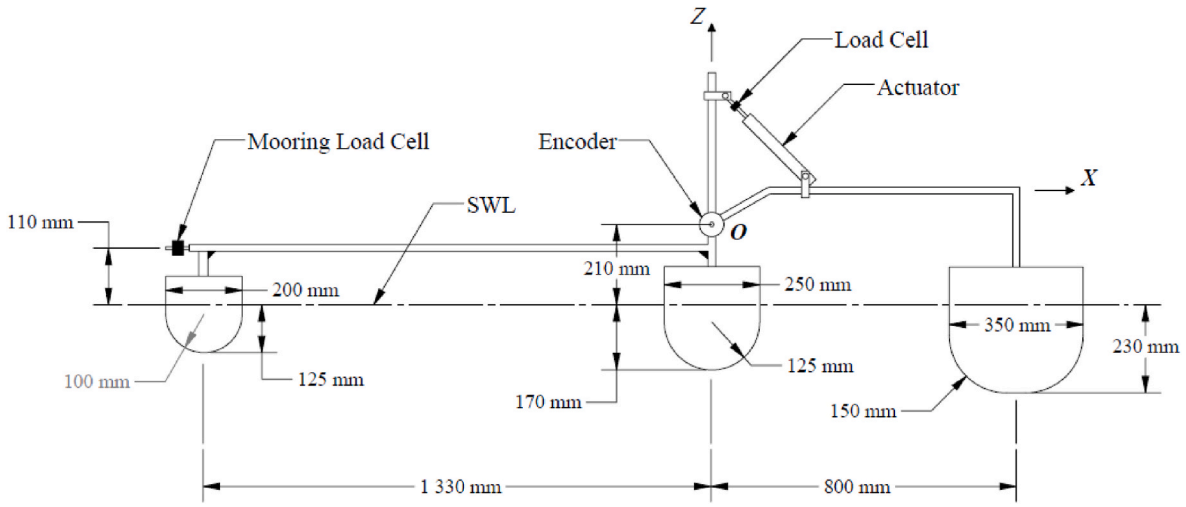

Fig. 2. Elevation of M4 system with dimensions (Moreno and Stansby, 2019).

Table 1
Properties of M4 scaled model.

	Front buoy	Middle buoy	Beam buoy
Mass (kg)	2.8	6.2	17.5
Mass centre position on z-direction (m)	−0.048	−0.067	−0.09
Radius of gyration Rx (m)	0.055	0.071	0.101
Radius of gyration Ry (m)	0.055	0.071	0.101
Radius of gyration Rz (m)	0.065	0.082	0.116

findings from these experiments are used in this study to validate and calibrate the Orcaflex model.

2.2.2. *Mooring system configuration*

In contrast to other offshore floating structures, the mooring system for WECs requires a balance between reliability and energy output. A poorly designed mooring system could decrease the energy conversion efficiency of a WEC, making it less cost-effective. Recent evidence suggests hybrid mooring systems outperform their single-mooring counterparts in WEC applications (Harris et al., 2004). As such, the scaled M4's mooring system is specifically designed to accommodate two mooring lines and a surface buoy in a configuration known as a slack moored system, as depicted in Fig. 3. The mooring line that connects the surface buoy to the basin floor is referred to as the bottom line, while the remaining line is termed the upper line.

The surface buoy weighs 87 g, and its dimension is relatively small compared to the M4 scaled model. So, the Morison equation calculated the hydrodynamic response of this surface buoy (Aamo and Fossen, 2000) rather than the diffraction analysis under the frequency domain. For the mooring line, the drag force is considered by the same approach as the crossflow principle. The fluid velocity relative to the line is split into its components $\mathbf{v_n}$ and $\mathbf{v_z}$ normal and parallel to the line axis. The drag force normal to the line axis is then determined by $\mathbf{v_n}$ and its x- and y-components v_x and v_y; the drag force parallel to the line axis is determined by $\mathbf{v_z}$. The drag force are calculated by the drag coefficients, C_{Dx}, C_{Dy} and C_{Dz}, and the drag areas appropriate to each direction.

$$f_{dx} = \frac{1}{2} p \rho d_n l C_{Dx} v_x |\mathbf{v_n}| \tag{2}$$

$$f_{dy} = \frac{1}{2} p \rho d_n l C_{Dy} v_y |\mathbf{v_n}| \tag{3}$$

$$f_{dz} = \frac{1}{2} p \rho \pi d_a l C_{Dz} v_z |v_z| \tag{4}$$

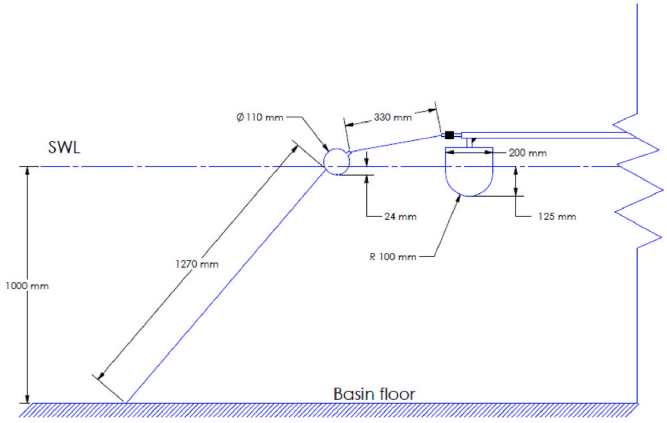

(a)

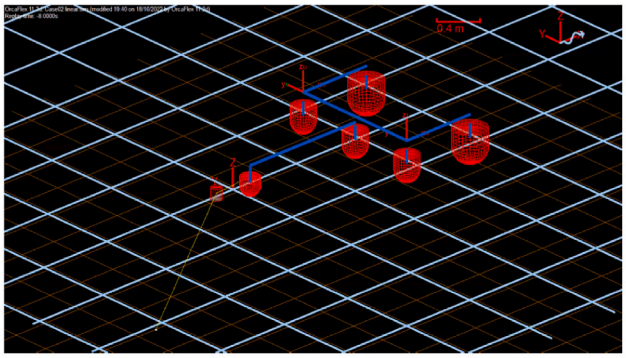

(b)

Fig. 3. The mooring configuration: (a). M4 scaled mode (Moreno and Stansby, 2019); (b) Orcaflex model.

Where p is proportion wet, ρ is the water density, d_n the normal drag diameter, l is the length of line represented by the node. d_a is the axis drag diameter.

The tension on the mooring line is calculated by its stiffness k, and strain. The nonlinear stiffness design is believed to reduce the peak load on the mooring line (Thies et al., 2014). Therefore, the bottom line used

in the basin test has a nonlinear stiffness shown in Fig. 4. Another two mooring lines with different stiffness curves are also selected in the numerical model to supply the comparison research. Cable 1, utilised in the basin experiment (named by E2), serves as the bottom mooring line. It features neutral buoyancy, floating with a slight volume above the water and a minimal dry mass. The specific material of the bungee cord is not explicitly known due to the proprietary secret. But its physical properties, including the stiffness information, are known. Other details can be found in the previous experimental study (Stansby et al., 2022). Cable 2 functions as a linear mooring cable comprising Polyester, a selection made from the OrcaFlex database to satisfy stiffness requirements. Cable 3, known as the Exeter tether (shown in Fig. 5), is a product of the University of Exeter. Its structure includes a hollow braided rope as an outer layer and load carrier, a radially compressible core functioning as an elastic hysteretic damper, and an anti-friction screen sandwiched in-between. This unique design allows the Exeter tether to exhibit variable stiffness in response to different tensile loads (Gordelier et al., 2015). Generally, nonlinear mooring lines can have different stiffness performances with varying damper configurations (Pecher et al., 2014). Nonlinear mooring lines also can enhance the survivability of the WECs under harsh marine conditions. They are designed to handle substantial displacements and deformations, thereby ensuring the WEC's safety and effective operation even under severe wave conditions. Moreover, the tension in the mooring doesn't increase linearly with extension owing to factors such as elasticity, weight, hydrodynamic loading, among others. By incorporating these nonlinear aspects, the Orcaflex can get more accurate predictions of the WEC's dynamic response. So, the comparison study between cable 1 and cable 3 cases would be helpful for the design of dynamic/passive damper used in the nonlinear mooring system. The upper mooring line's properties are linear and maintain the same in all cases. Other properties of mooring cables are shown in Table 2.

3. Comparison of the simulation and basin test

The potential flow theory has some limitations in handling the floating structures' large motion amplitude under the time domain owing to the mean wet surface used in the diffraction analysis. Based on the Orcaflex manual, " … When diffraction analysis data are used in OrcaFlex, these two approaches are in conflict: the diffraction analysis approach says that the wave height is so small that the loads applied to the vessel are tiny and it therefore does not move, but the time-domain method, using full wave height, is continually updating the loads as the vessel moves in response to those very same loads. The greatest risk is that quadratic loading on a vessel is applied twice: once by use of QTF data, and once by applying the linear diffraction analysis loads using the instantaneous state of the system. Orcaflex refers to this as double-counting part of the loading defined by QTF data … " (Orcina, 2022).

To address this numerical issue, OrcaFlex applies two methods, Filtering and QTF modifications, to remove the second-order loading contributions which arise naturally in the time domain. The principle of these two methods is: i) The Filtering model avoids the contributions arising in the time domain model via filtering/dividing the floater motion into wave response motion and low-frequency motion; ii) The QTF modification model can allow the contributions to arise naturally in the time domain model, but remove them from the second order loads. More details of the difference between the two approaches can be found in the Appendix.

The Filter and QTF modification methods should yield similar hydrodynamic responses for a simple-structure floating body interacting with small-scale waves. However, the difference between the outcomes of these two methods may become more pronounced when dealing with complex structures and larger waves. Consequently, this section will compare the numerical findings of both methods against experimental results to identify the most fitting simulation approach for the M4 WEC.

The wave conditions used in the numerical model are defined by the JONSWAP spectrum with spectral peakedness $\gamma = 3.3$ and 1 m water depth, identical to the basin test (Table 3). Additionally, the simulation time of each case is 600s, also matching the experimental configurations. However, the simulation includes an extra 8s (from -8s to 0s) to start up the simulation gradually. In addition, the explicit calculation with "always use the recommended time step" is selected for better solution convergence. More details of the explicit method can be found in Manual, (2012).

The tension loading outcomes for the bottom mooring line are displayed in Fig. 6. A review of the data reveals that both computational methods align reasonably well with the experimental results. The difference between the two numerical methods is negligible for the average tension results when wave heights are small (as seen in case 1 to case 4). Nevertheless, these differences begin to grow under conditions of larger waves (case 5 to case 7), with the Filter model significantly outperforming the QTF model in terms of tension prediction. When it comes to maximum tension, both numerical models considerably underestimate the results. This discrepancy may be attributable to two factors: i) wave overtopping and ii) reflected waves from the beach during the experiment. The wave overtopping could result in additional downward pressure and an increase in the tensile load on the mooring line. The wave reflections, which the numerical model couldn't consider, could be significant enough over the 600s time-length to account for the divergence between numerical and experimental results.

As shown in Fig. 7, the Filter model also performs better in the rotation results from prediction, except for the max rotation results in

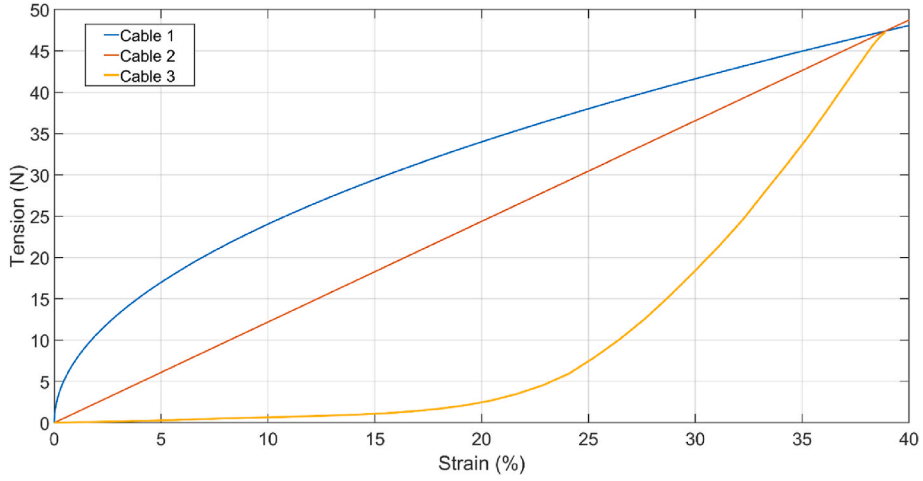

Fig. 4. The stiffness curve of the three cables in the numerical model, cable 1 is also used in the basin test.

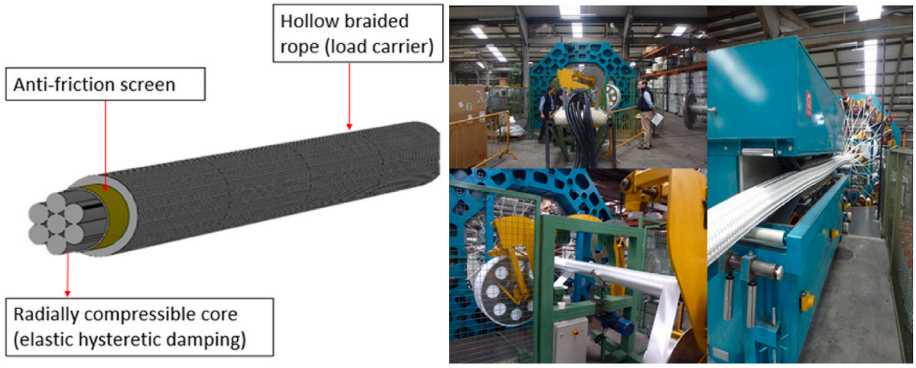

Fig. 5. The concept and manufacture of the Exeter tether.

Table 2
The properties of mooring cables.

	Stiffness (N/m)	Diameter (m)	Mass (kg/m)
Upper mooring line	98.37e3	0.0082	0.072
Bottom mooring line (cable 1)	Shown in Fig. 4	0.008	0.05
Bottom mooring line (cable 2)		0.008	0.05
Bottom mooring line (cable 3)		0.008	0.05

Table 3
The wave conditions.

Case	Significant Wave height Hs (m)	Peak Wave Period (s)
1	0.057	1
2	0.059	1.2
3	0.057	1.4
4	0.056	1.8
5	0.116	1.2
6	0.142	1.4
7	0.144	1.8

case 5. The Filter model overestimated the rotation amplitude up to 50%. According to Fig. 7 (a), the peak relative rotation amplitude would appear at between 1.2s and 1.4s, which means the natural period of the M4 scaled model may locate in this range. As a result, the numerical errors were relatively more significant in these cases.

The PTO used in the basin test is a pneumatic cylinder damper, supplying an approximate linear damping. Limited by the experimental conditions, the PTO was only engaged in the small/moderate wave cases. Additionally, the differences caused by the two simulation approaches are not significant under the operational waves. Therefore, only the filter model was selected in the PTO case comparisons. The H_s in the PTO cases is 0.04 m, and T_p ranges from 1s to 1.8s. The average power results comparisons are shown in Fig. 8. It was found that the results from the Orcaflex and basin test followed the same trend. Similar to the non-PTO cases, the Orcaflex underestimated the average output power, and the differences were more significant when the wave periods were shorter than 1.4s. The linear model in the previous study also underestimated by up to 30% around 1.4 s but showed close agreement for larger Tp (Moreno and Stansby, 2019).

As illustrated in Figs. 6 and 7, the Orcaflex corresponds well with the experimental outcomes under small wave conditions but shows a less satisfying correlation under severe wave conditions. This discrepancy is attributed to the potential flow limitations when there is a significant change in the buoy's wet surface. The latter provides superior predictions in all mean results when comparing the QTF and Filter methods. Although the QTF shows marginally better performance predicting the maximum tension results, the difference is insignificant. Consequently, given these considerations, the Filter method is the preferred choice for this study.

4. Results

This section presents the numerical simulation's main results, including i) tensile load on the bottom lines, ii) the M4 motion, and iii) an initial adjustment of cable 3 stiffness properties.

4.1. Tensile load on the bottom mooring line

As described in Section 2, the bottom line is designed with three varying stiffness levels. To facilitate a more effective comparison, the results within the frequency domain are categorised into three groups, as

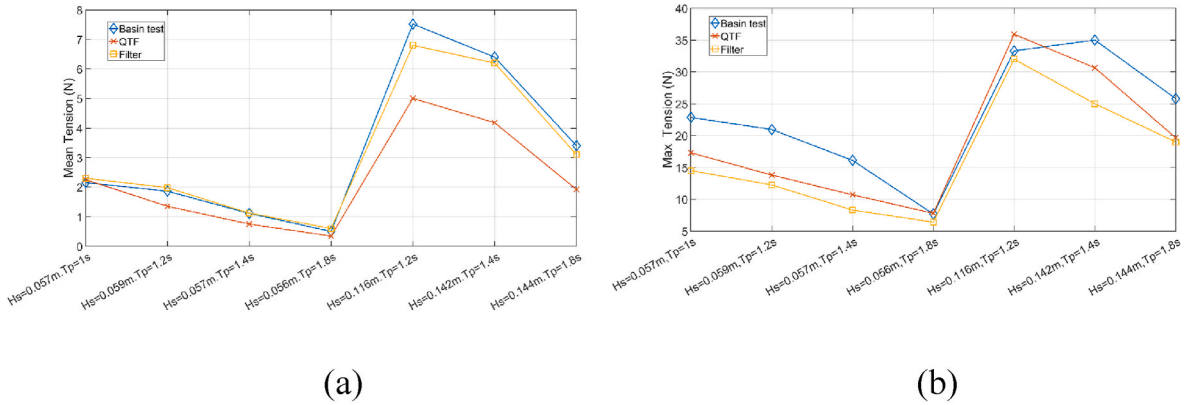

Fig. 6. The tension on the bottom mooring line in the numerical and experimental models: (a) mean tension, (b) max tension.

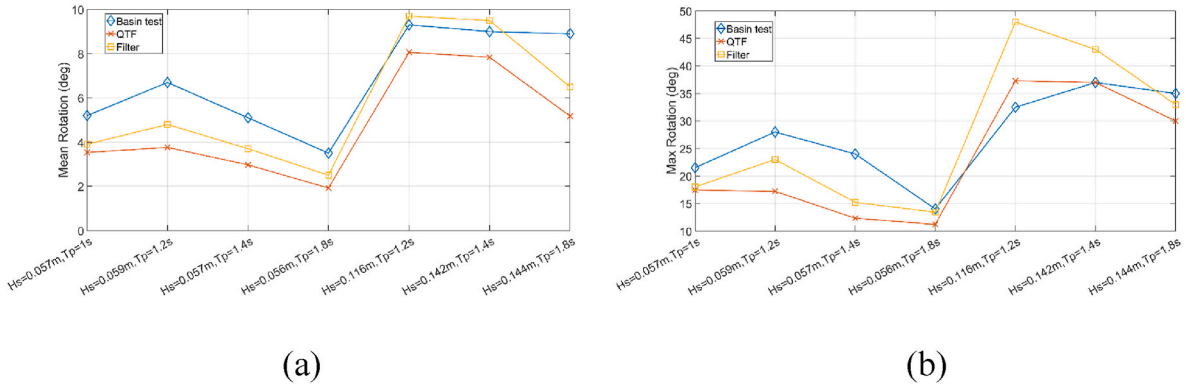

Fig. 7. The relative rotation degree in the numerical and physical model: (a) Mean, (b) Max.

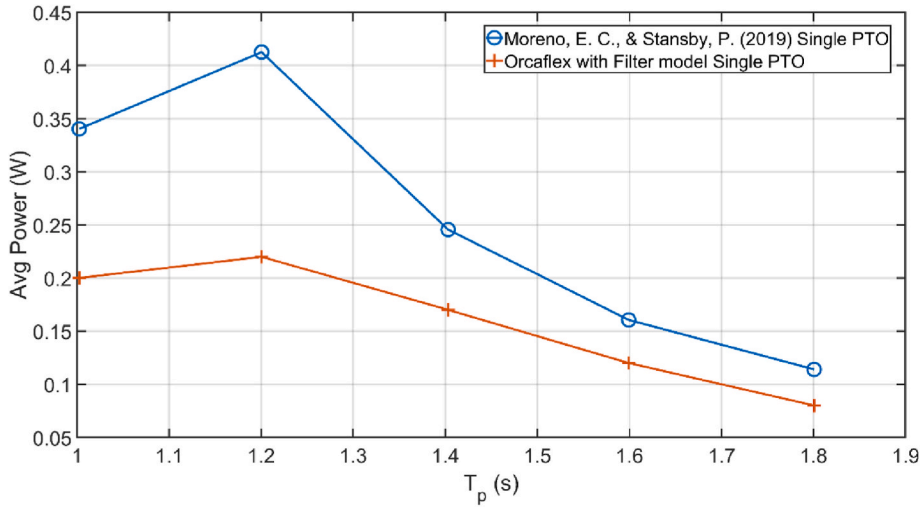

Fig. 8. The PTO cases comparison between Orcaflex and the basin test for single PTO.

shown in Fig. 9. The first group, or Fig. 9a, consists of cases with small significant wave heights (approximately 0.057 m) and varying peak wave periods (ranging from 1s to 1.8s). Fig. 9b presents the results with a relatively higher wave height (0.143 m) and peak wave periods of 1.4s and 1.8s. Fig. 9c illustrates the comparative results between different wave heights and identical wave periods. Two peaks can be identified in the tension frequency results, attributed to low-frequency drifting and wave response. Given that low-frequency drifting can cause a substantial offset for the scaled model, the low-frequency peak exhibits a higher spectral density. Furthermore, the experimental results in the frequency domain also recognise the peak due to low-frequency drifting, thereby validating the numerical model, as observed in Fig. 10.

Moreover, these two peaks can be influenced by the properties of the mooring line. For the wave response peak, the spectral densities were considerably reduced by cables 2 & 3, with cable 3 providing the lowest density. For the low-frequency peak, both the peak frequency and spectral density are affected by these three cables, but no specific cable can be seen to consistently reduce the peak amplitude across all cases. Nevertheless, cable 3 consistently offers the relatively smallest spectral density and the lowest peak occurrence frequencies in all instances.

It is worth mentioning that the spectral density of tension can only reflect the mean tension load on the mooring cable rather than the maximum tension. With this consideration, Fig. 11 shows the mean and maximum tension in cases 4 & 5. It is found that the mean tension of cable 3 is smaller than the other two cables in both cases. The largest maximum tension is observed on cable 3 in case 5, which is caused by the large motion of the model (shown in Figs. 11 and 7). According to Fig. 4, the tension (stiffness) of cable 3 sharply increases when its strain exceeds 35%.

4.2. Motion characteristics

The relative movement between the four front/mid buoys and the two rear buoys is crucial to the design of the M4, especially concerning the position and constraints of the joint structure. The effects of different mooring cables on relative motion are depicted in Fig. 12. Echoing the tension results, cases 4 and 5 are chosen for illustration. No noticeable differences in relative motion caused by varying mooring cables are detected. The most significant discrepancy is less than 5% for both mean and max results, which suggests that the different mooring cables will exert a negligible impact on the installation and connection design of the M4.

Contrary to the rotation motion, the mooring cable significantly affects the translational motion. In case 4 (Fig. 13a), the strain imposed on the bottom mooring cable by the device is minimal. Cable 3 is quite flexible, with its slight strain leading to a relatively larger offset and reduced tension. However, under more severe wave conditions (Fig. 13b), the tension in cable 3 dramatically escalates once the device offset surpasses 0.6 m due to its rapidly increasing stiffness.

It is also observed that the maximum tension does not coincide with the device's largest offset, especially under large wave conditions (as in case 5). This is because the motion under other degrees of freedom can

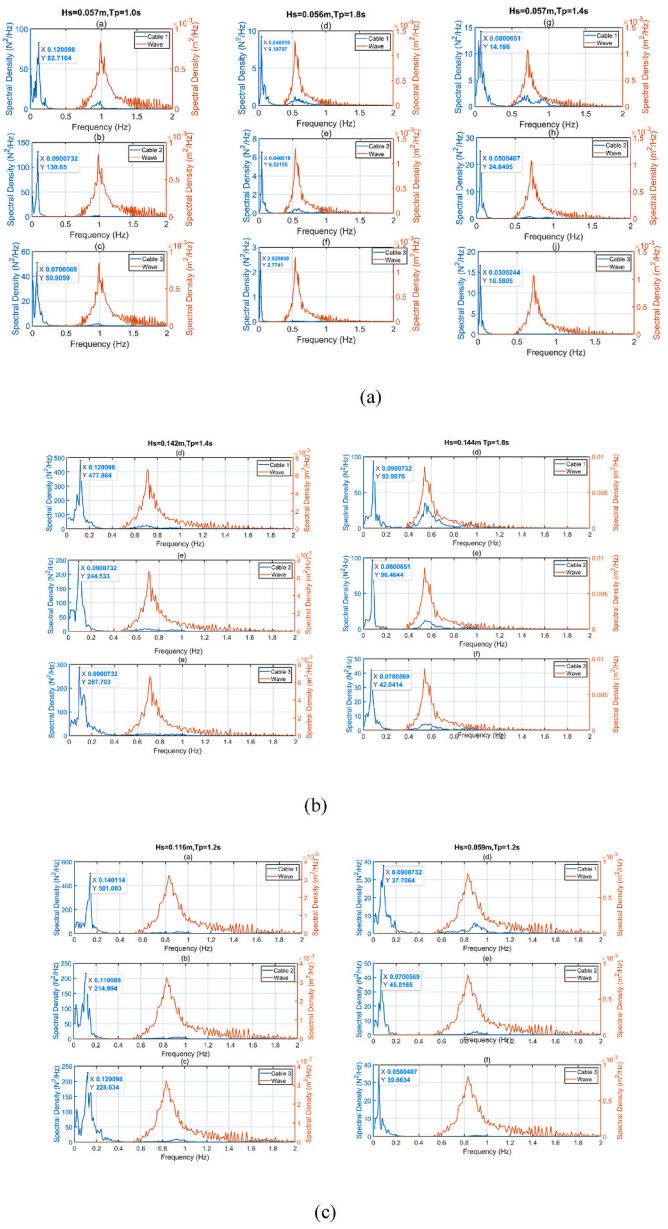

Fig. 9. The tensile load of the bottom line under the frequency domain, cable 1 has the same stiffness characteristic as in the basin test.

primarily contribute to cable strain. The results in Fig. 14 reveal that the peak tension occurs in conjunction with the largest heave motion of the front buoy, rather than the model's x-offset, around 300 s.

4.3. Cable 3 properties adjustment

The frequency-domain tension results (Fig. 9) highlight the benefits of cable 3 in tension reduction. However, time domain results (Fig. 13) reveal that the current cable 3 tends to be overly flexible under low-tension loading and excessively stiff under high-tension loading. Therefore, we adjusted the stiffness properties of cable 3 in this section. It's crucial to note that this adjustment aims to demonstrate the potential of cable 3 (or cables with similar stiffness properties) in tension and drift reduction, not to quantify the optimal properties.

The approach to adjusting the stiffness properties is threefold: i) Fit a curve to the current stiffness properties; ii) Adjust the curve parameter based on time-domain results and engineering constraints; iii) Implement the new properties in the numerical model and compare the device motion characteristics. Here, the stiffness curve of cable 3 was fitted using the 2nd polynomial method ($y = ax^2+bx + c$), yielding an R-square value of 0.987 (Table 4 and Fig. 15). As shown in Table 4, the c is limited to zero, and we increase the a, b to change the bending of the new cable 3's stiffness curve.

The offset and tension change caused by the stiffness adjustment are shown in the figure. Under the small wave case (Fig. 16 a), the new cable 3 can reduce around 30% maximum offset distance with a similar peak tension. The advantages caused by the stiffness adjustment are more significant under large wave cases (Fig. 16 b), with a 50% peak tension reduction and a 10% offset distance decrease.

5. Discussions

This study provided insights into the performance of the SPM mooring system in a M4 6-float WEC. Using OrcaFlex simulations, the study could accurately simulate various nonlinear patterns for the mooring lines. The findings from this study underscore the complexity of the interactions between the WEC and its mooring system and highlight the importance of comprehensive and multifaceted evaluations in optimising these systems.

One of the significant findings of this study was the impact of cable stiffness on the tension load of the mooring system. Specifically, cable 3, characterised by its negative bending, consistently displayed the smallest spectral density and the lowest peak occurrence frequencies across all cases. Despite this, cable 3 also demonstrated the largest maximum tension in some cases, indicating the need for its stiffness to be optimised to improve its performance under a range of wave conditions. This discovery suggests that while certain cables may be advantageous in some aspects, such as tension reduction, they may also present challenges in others, such as handling high-tension loads. Therefore, a balance needs to be struck when choosing the mooring cables for a WEC.

Another key finding was that different mooring cables had a negligible impact on the relative motion between the buoys of the M4. This suggests that the design of the installation and connection of the M4 can be relatively independent of the mooring cable choice. However, the mooring cable significantly affected the translational motion, emphasising the complexity of the interactions between the mooring system and the device dynamics.

Interestingly, the study found that the maximum tension did not always occur at the device's largest offset, especially under larger wave conditions. This implies that other factors, beyond just the device's offset, can contribute significantly to cable strain. This discovery highlights the need for comprehensive assessments that take into account a wide range of factors when evaluating the performance of a mooring system.

The study also investigated the performance of the newly adjusted cable 3, which reduced up to 30% of the maximum offset distance and similar peak tension in small wave cases. This suggests that adjusting the stiffness properties of mooring cables might be a promising approach to optimising the performance of WECs.

In conclusion, this study offers critical insights into the dynamics of a multi-float hinged WEC with a nonlinear mooring system. The findings underscore the importance of selecting the right mooring cables and adjusting their properties to optimise the performance of the WEC. Future research could explore the long-term performance and durability of different mooring cables under a range of operational conditions, as well as further optimisation of stiffness properties for tension reduction and performance enhancement.

6. Conclusions

This research examined the hydrodynamic and energy output performance of the M4 WEC employing different mooring cables (two nonlinear and one linear mooring cable). The primary conclusions

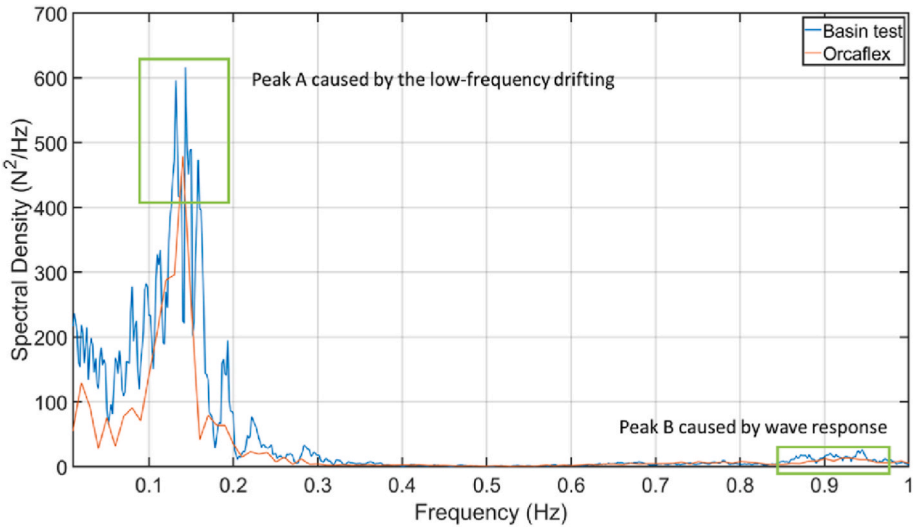

Fig. 10. The comparison of Orcaflex and Basin test mooring force frequency-domain results, Hs = 0.116 m. Tp = 1.2s.

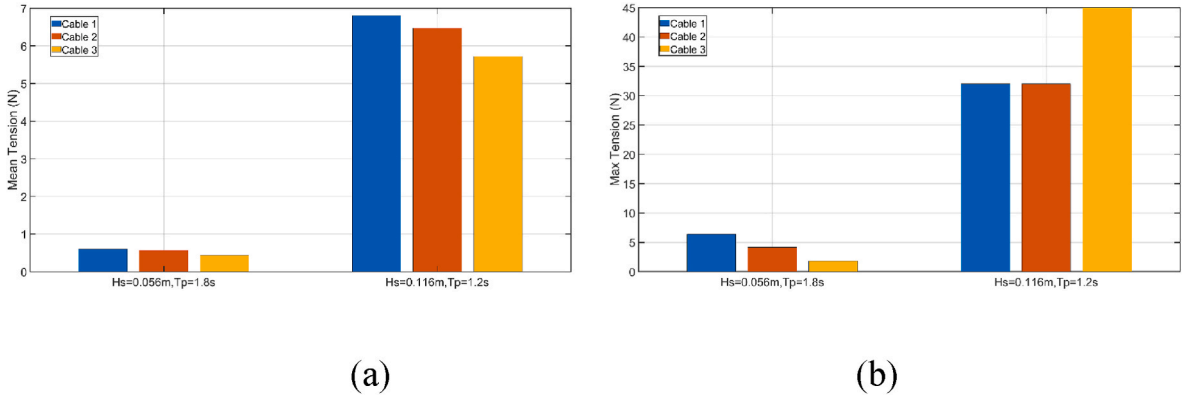

Fig. 11. The mean and maximum tension in case 4&5:(a) mean tension, (b) maximum tension.

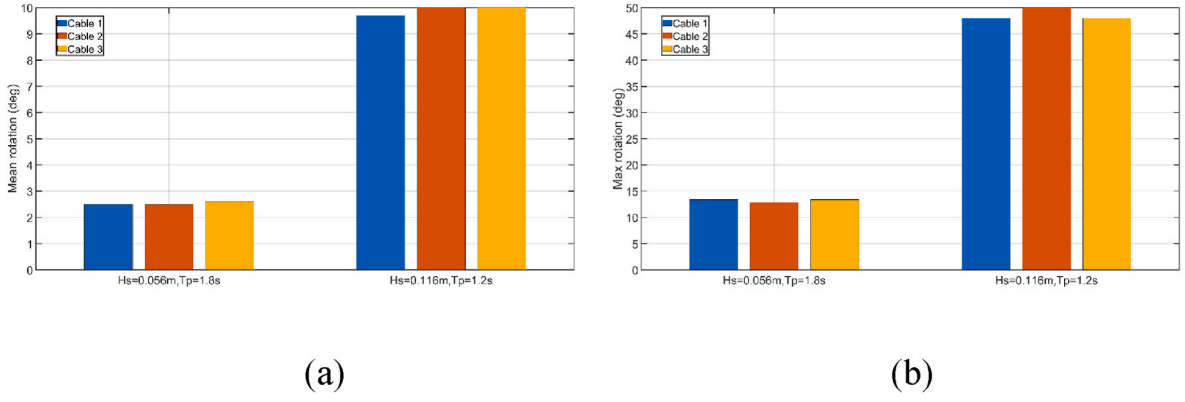

Fig. 12. The mean and maximum rotation in cases 4&5: (a) mean rotation, (b) max rotation.

drawn are as follows:

a. Significant discrepancies may arise from the two simulation methodologies provided by OrcaFlex. Given this, comparison research is strongly recommended when floating bodies are anticipated to encounter large motion amplitudes. For this study, the filter method aligns more closely with experimental results than the QTF method.

b. The nonlinear mooring components predominantly impact the tensile load resulting from the first-order wave response. Mooring cables exhibiting a negative bending stiffness curve (where the curvature of the stiffness curve is negative, as in cable 3 in this study) provide the best reduction in mean tension.

c. Both the tension and the device's offset are influenced by the stiffness properties of the mooring cable. In this study, cable 3 was too flexible under light loads and overly rigid under high loads. The stiffness

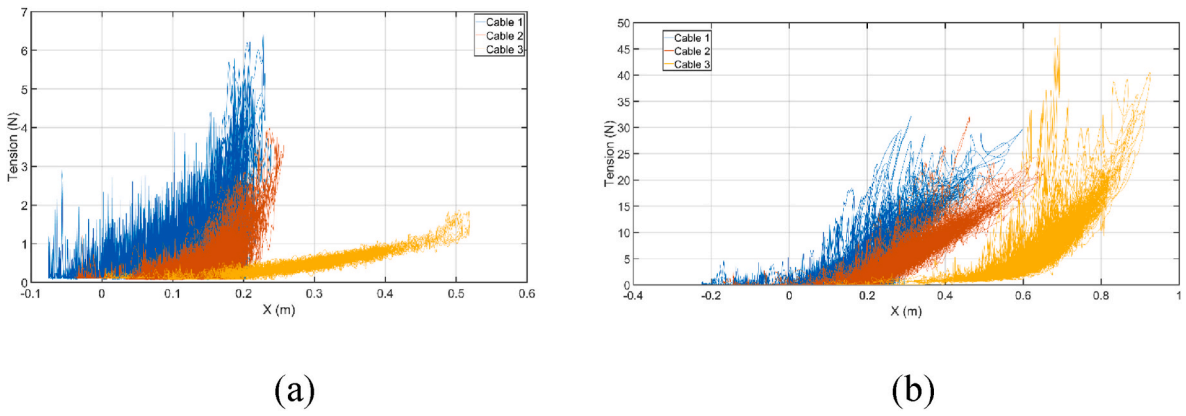

Fig. 13. The tension of bottom cable vs device offset: (a) Case 4, (b) Case 5.

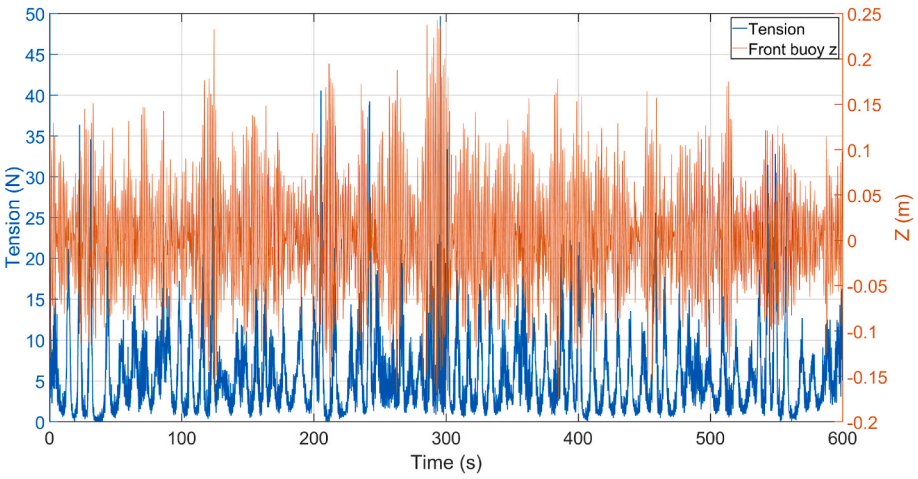

Fig. 14. The tension of cable 3 and the heave displacement of front buoy in case 5.

Table 4
Cable 3 stiffness curve fitness.

	Cable 3 before adjustment	Cable 3 after adjustment
Fitted curve	y = 0.06425x^2-1.493x+7.065	y = 0.332x^2-0.06397x
R-square	0.987	N/A

properties of cable 3 were modified by altering the parameters of the fitted stiffness curve. The adjusted cable 3 can decrease the offset distance by up to 30% and the peak tension by 50%.

d. The relative pitch motion between the front and rear buoy of the M4 (from which the PTO system extracts energy) is not sensitive to the stiffness properties of the mooring cable.
e. The nonlinear mooring components primarily affect the M4's drifting offset rather than its relative rotation motion.

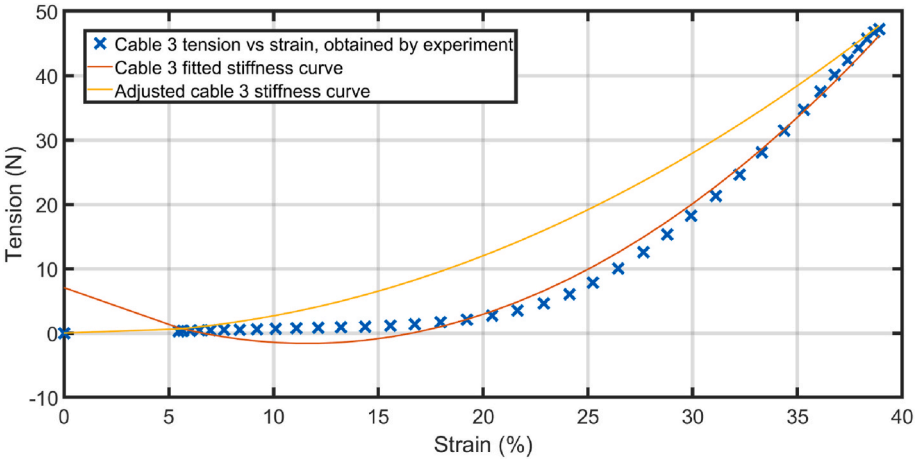

Fig. 15. Cable 3 stiffness adjustment.

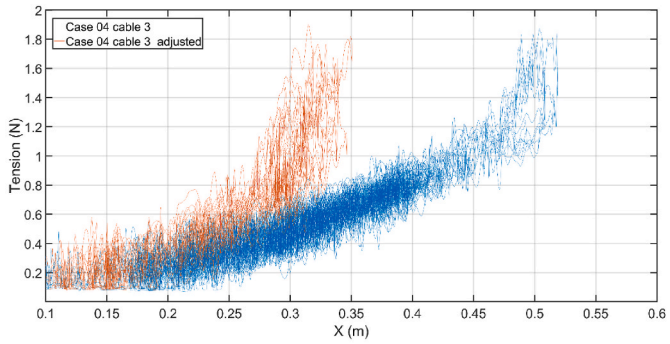

(a)

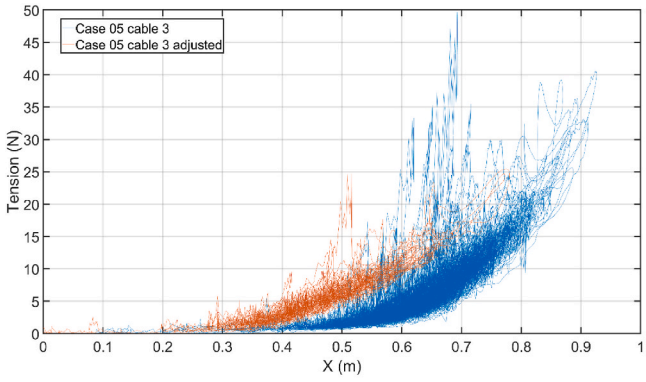

(b)

Fig. 16. The tension of new cable 3 vs device offset: (a) Case 4, (b) Case 5.

CRediT authorship contribution statement

Chenyu Zhao: Writing – original draft, Preparation, Writing – review & editing. **Peter Stansby:** Writing – review & editing, Supervision, Project administration, Funding acquisition. **Lars Johanning:** Methodology, Supervision, Writing – review & editing.

Declaration of competing interest

The authors declare that they have no known competing financial interests or personal relationships that could have appeared to influence the work reported in this paper.

Data availability

Data will be made available on request.

Acknowledgements

Support for Lir ocean basin access through the EU Marinet2 programme for this project M4moor (reference number 5031) and for funding through the EPSRC MoorWEC grant EP/V039946/1 is gratefully acknowledged.

Appendix

Prevention using filtering approach

OrcaFlex can follow the example set by diffraction analysis, and limit the interaction between vessel loading and response.

- Rotation of applied load components out of the horizontal plane is ignored by use of heading frames when appropriate.
- The vessel motion is filtered to remove the instantaneous wave frequency response, and that filtered motion can be used as an appropriate input when updating diffraction analysis loads.

When OrcaFlex applies diffraction loads using these filtered responses, only the provided QTF data contributes any nonlinear load from diffraction effects. In some simulations, Filtering the frequency content of instantaneous response may be difficult in the time domain, and it is difficult to achieve perfect separation of loading and response.

Prevention using QTF modification approach

OrcaFlex can also prevent double-counting of QTF loads by filtering the diffraction analysis results, instead of the time domain behaviour. Perfect filtering can be achieved in diffraction analysis, because it is conducted in the frequency domain, and the filtering is implemented in OrcaFlex by simply subtracting common second order loads from the input QTF data. Common second order loads are those which arise from more than one source (we use "common" here in the sense of shared, not frequently-occurring): they appear as part of the time domain analysis when linear diffraction analysis loads are applied using the instantaneous state of the system, and also contribute to the QTF data calculated in diffraction analysis.

With this subtraction of the common terms from the original QTF data, OrcaFlex can now therefore apply diffraction data using the instantaneous state of the system without incorrectly duplicating the higher-order effects. Common nonlinear effects that were previously truncated to the quadratic term present in the QTF data are now fully represented during a simulation.

References

Aamo, O.M., Fossen, T.I., 2000. Finite element modelling of mooring lines. Math. Comput. Simulat. 53 (4–6), 415–422.
Aderinto, T., Li, H., 2018. Ocean wave energy converters: status and challenges. Energies 11 (5), 1250.
Ahamed, R., McKee, K., Howard, I., 2020. Advancements of wave energy converters based on power take off (PTO) systems: a review. Ocean. Eng. 204, 107248.
Antonio, F.d.O., 2010. Wave energy utilization: a review of the technologies. Renew. Sustain. Energy Rev. 14 (3), 899–918.
Astariz, S., Iglesias, G., 2015. The economics of wave energy: a review. Renew. Sustain. Energy Rev. 45, 397–408.
Cambridge, U.o., 2023. The stiffness of rubber. https://www.doitpoms.ac.uk/tlplib/stiffness-of-rubber/printall.php.
Clément, A., McCullen, P., Falcão, A., Fiorentino, A., Gardner, F., Hammarlund, K., Lemonis, G., Lewis, T., Nielsen, K., Petroncini, S., 2002. Wave energy in Europe: current status and perspectives. Renew. Sustain. Energy Rev. 6 (5), 405–431.
Fonseca, N., Pascoal, R., Morais, T., Dias, R., 2009. Design of a mooring system with synthetic ropes for the FLOW wave energy converter. Int. Conf. Offshore Mech. Arctic Eng. 1189–1198.
Gordelier, T., Parish, D., Thies, P.R., Johanning, L., 2015. A novel mooring tether for highly-dynamic offshore applications; mitigating peak and fatigue loads via selectable axial stiffness. J. Mar. Sci. Eng. 3 (4), 1287–1310.
Harris, R.E., Johanning, L., Wolfram, J., 2004. Mooring Systems for Wave Energy Converters: A Review of Design Issues and Choices. Marec2004.
Huang, S., Sheng, S., You, Y., Gerthoffert, A., Wang, W., Wang, Z., 2018. Numerical study of a novel flex mooring system of the floating wave energy converter in ultra-shallow water and experimental validation. Ocean. Eng. 151, 342–354.
Liao, Z., Stansby, P., Li, G., Moreno, E.C., 2021. High-capacity wave energy conversion by multi-float, multi-pto, control and prediction: generalized state-space modelling with linear optimal control and arbitrary headings. IEEE Trans. Sustain. Energy 12 (4), 2123–2131.
Liu, Z., Qu, N., Han, Z., Zhang, J., Zhang, S., Li, M., Shi, H., 2016. Study on energy conversion and storage system for a prototype buoys-array wave energy converter. Energy Sustain. Dev. 34, 100–110.
López, I., Andreu, J., Ceballos, S., De Alegría, I.M., Kortabarria, I., 2013. Review of wave energy technologies and the necessary power-equipment. Renew. Sustain. Energy Rev. 27, 413–434.
Manual, O., 2012. Online at. http://www.orcina.com/SoftwareProducts/OrcaFlex/Documentation.OrcaFlex.pdf.
Manual, O.U., 2006. Orcina Ltd. Daltongate, UK.

Moreno, E.C., Stansby, P., 2019. The 6-float wave energy converter M4: ocean basin tests giving capture width, response and energy yield for several sites. Renew. Sustain. Energy Rev. 104, 307–318.
Orcina, 2022. Calculation model. . https://www.orcina.com/webhelp/OrcaFlex/Default_Left.htm#StartTopic=html/Vesseldata,Calculationdata.htm|SkinName=Web%20Help.
Orcina, L., 2016. OrcaFlex User Manual Version 11.0 B. Orcina Ulverston, UK.
Pacaldo, J.C., Bilgera, P.H.T., Abundo, M.L.S., 2022. Nearshore wave energy resource assessment for off-grid Islands: a case study in cuyo Island, Palawan, Philippines. Energies 15 (22), 8637.
Pecher, A., Foglia, A., Kofoed, J.P., 2014. Comparison and sensitivity investigations of a CALM and SALM type mooring system for wave energy converters. J. Mar. Sci. Eng. 2 (1), 93–122.
Shi, X., Liang, B., Du, S., Shao, Z., Li, S., 2022. Wave energy assessment in the China East Adjacent Seas based on a 25-year wave-current interaction numerical simulation. Renew. Energy 199, 1381–1407.
Stansby, P., Draycott, S., Li, G., Zhao, C., Moreno, E.C., Pillai, A., Johanning, L., 2022. Experimental study of mooring forces on the multi-float WEC M4 in large waves with buoy and elastic cables. Ocean. Eng. 266, 113049.
Stansby, P., Moreno, E.C., Stallard, T., Maggi, A.J.R.E., 2015. Three-float Broad-Band Resonant Line Absorber with Surge for Wave Energy Conversion, vol. 78, pp. 132–140.
Sun, P., Li, Q., He, H., Chen, H., Zhang, J., Li, H., Liu, D., 2021. Design and optimization investigation on hydraulic transmission and energy storage system for a floating-array-buoys wave energy converter. Energy Convers. Manag. 235, 113998.
Thies, P.R., Johanning, L., McEvoy, P., 2014. A novel mooring tether for peak load mitigation: initial performance and service simulation testing. Int. J. Mar. Energy 7, 43–56.
Thomsen, J.B., 2015. Mooring solutions for large wave energy converters. In: International Network on Offshore Renewable Energy (INORE): 11th International Symposium.
Thomsen, J.B., Ferri, F., Kofoed, J.P., 2015. Assessment of Current State of Mooring Design in the Danish Wave Energy Sector, European Wave and Tidal Energy Conference. Technical Committee of the European Wave and Tidal Energy Conference, 08B05-05-01.
Wang, W., Zhao, C., Peng, W., Ding, W., Chen, M., Li, Y., Johanning, L., 2022. Nonlinear mooring system for a 'Sharp-Eagle' wave energy converter. Ocean. Eng. 260, 111970.
Weller, S., Davies, P., Vickers, A., Johanning, L., 2015a. Synthetic rope responses in the context of load history: the influence of aging. Ocean. Eng. 96, 192–204.
Weller, S., Johanning, L., Davies, P., Banfield, S., 2015b. Synthetic mooring ropes for marine renewable energy applications. Renew. Energy 83, 1268–1278.
Xu, S., Soares, C.G., 2020. Experimental investigation on short-term fatigue damage of slack and hybrid mooring for wave energy converters. Ocean. Eng. 195, 106618.
Xu, S., Wang, S., Soares, C.G., 2019. Review of mooring design for floating wave energy converters. Renew. Sustain. Energy Rev. 111, 595–621.
Yang, C., Xu, T., Wan, C., Liu, H., Su, Z., Zhao, L., Chen, H., Johanning, L., 2022. Numerical investigation of a dual cylindrical OWC hybrid system incorporated into a fixed caisson breakwater. Energy, 126132.
Zhao, C., Thies, P.R., Johanning, L., 2021a. Investigating the winch performance in an ASV/ROV autonomous inspection system. Appl. Ocean Res. 115, 102827.
Zhao, C., Thies, P.R., Ye, Q., Lars, J., 2021b. System integration and coupled effects of an OWT/WEC device. Ocean. Eng. 220, 108405.